1521-0111/100/1/63–72$35.00
MOLECULAR PHARMACOLOGY

https://doi.org/10.1124/molpharm.120.000231
Mol Pharmacol 100:63–72, July 2021

Antitumor Activity of Novel Signal Transducer and Activator of Transcription 3 Inhibitors on Retinoblastoma

Dong Hyun Jo[1], Seungbeom Lee[1], Eunoo Bak[1], Chang Sik Cho, Young Taek Han, Kyeojin Kim, Young-Ger Suh, and Jeong Hun Kim

Department of Anatomy and Cell Biology (D.H.J.) Department of Ophthalmology (E.B., J.H.K.), and Department of Biomedical Sciences (J.H.K.), Seoul National University College of Medicine, Seoul, Republic of Korea; College of Pharmacy, CHA University, Pocheon-si, Republic of Korea (S.L., K.K., Y.-G.S.); Fight against Angiogenesis-Related Blindness (FARB) Laboratory, Biomedical Research Institute, Seoul National University Hospital, Seoul, Republic of Korea (C.S.C.); and College of Pharmacy, Dankook University, Cheonan-si, Republic of Korea (Y.T.H.)

Received December 29, 2020; accepted April 13, 2021

ABSTRACT

Signal transducer and activator of transcription 3 (STAT3) is a plausible therapeutic target in the treatment of retinoblastoma, the most common intraocular malignant tumor in children. STAT3, a transcription factor of several genes related to tumorigenesis, is activated in retinoblastoma tumors as well as other cancers. In this study, we investigated the structure-activity relationship of a library of STAT3 inhibitors, including a novel series of derivatives of the previously reported compound with a Michael acceptor (compound **1**). We chose two novel STAT3 inhibitors, compounds 11 and 15, from the library based on their inhibitory effects on the phosphorylation and transcription activity of STAT3. These STAT3 inhibitors effectively suppressed the phosphorylation of STAT3 and inhibited the expression of STAT3-related genes *CCND1*, *CDKN1A*, *BCL2*, *BCL2L1*, *BIRC5*, *MYC*, *MMP1*, *MMP9*, and *VEGFA*. Intraocularly administered STAT3 inhibitors decreased the degree of tumor formation in the vitreous cavity of BALB/c nude mice of an orthotopic transplantation model. It is noteworthy that compounds 11 and 15 did not induce in vitro and in vivo toxicity on retinal constituent cells and retinal tissues, respectively, despite their potent antitumor effects. We suggest that these novel STAT3 inhibitors be used in the treatment of retinoblastoma.

SIGNIFICANCE STATEMENT

The current study suggests the novel STAT3 inhibitors with Michael acceptors possess antitumor activity on retinoblastoma, the most common intraocular cancer in children. Based on detailed structure-activity relationship studies, we found a 4-fluoro and 3-trifluoro analog (compound 11) and a monochloro analog (compound 15) of the parental compound (compound 1) inhibited STAT3 phosphorylation, leading to suppressed retinoblastoma in vitro and in vivo.

Introduction

Signal transducer and activator of transcription 3 (STAT3) is a plausible target for the treatment of retinoblastoma, the most common intraocular cancer in children (Dimaras et al., 2015). It is noteworthy that STAT3 is activated in retinoblastoma tissues, especially with characteristics of advanced tumors (Mohan et al., 2006; Jo et al., 2014). Also, various therapeutic approaches showed that modulating STAT3 activation suppressed the proliferation and progression of retinoblastoma cells (Jo et al., 2014; Liu et al., 2016; Hu et al., 2018; Liang et al., 2018; Liu et al., 2018; Zhang et al., 2018; Sun et al., 2020). As in other cancers, targeting STAT3 is a feasible way to treat the patients with retinoblastoma (Yu et al., 2014; Johnson et al., 2018; Huynh et al., 2019). Current treatment options against retinoblastoma include intravenous chemotherapy, usually with a cocktail of vincristine, etoposide, and carboplatin, and intra-arterial chemotherapy based on melphalan and topotecan (Dimaras and Corson, 2019). These conventional drugs target microtubules (vincristine), topoisomerase (I, topotecan; II, etoposide), and DNA (carboplatin and melphalan). In this context, a targeted therapy inhibiting cancer-specific signaling pathways other than cellular proliferation machineries, such as the STAT3 pathway, might be of potential to suppress retinoblastoma tumors in coordination with currently available drugs.

We previously reported that a compound containing Michael acceptor (compound **1** in this study) directly binds to STAT3 and inhibits the transcription activity of STAT3, sup-

This work was supported by the Creative Materials Discovery Program through the National Research Foundation of Korea (NRF) funded by the Ministry of Science and ICT [2018M3D1A1058826]; the Global Core Research Center (GCRC) grant from the NRF/the Ministry of Education, Science and Technology, Republic of Korea [2012-0001187]; the Seoul National University Hospital Research Grant [04-2019-0280]; and the Basic Science Research Program through the NRF funded by the Ministry of Education [2017R1A6A3A04004741].

The authors have nothing to declare.

Primary laboratory of origin: Fight against Angiogenesis-Related Blindness (FARB) Laboratory, Biomedical Research Institute, Seoul National University Hospital, Seoul, Republic of Korea.

[1]D.H.J., S.L., and E.B. contributed equally to this work.

https://doi.org/10.1124/molpharm.120.000231.

ABBREVIATIONS: ATCC, American Type Culture Collection; d, doublet; GI_{50}, the concentrations at which a growth inhibition of 50% is achieved; HRMEC, human retinal microvascular endothelial cell; m, multiplet; s, singlet; SAR, structure-function relationship; STAT3, signal transducer and activator of transcription 3; t, triplet; TUNEL, terminal deoxynucleotidyl transferase dUTP nick-end labeling.

pressing the proliferation of several breast cancer cell lines (Kim et al., 2015). On the other hand, several analogs of the compound without a Michael acceptor failed to exhibit antiproliferative effects, which suggests that Michael acceptor is the crucial pharmacophore (Kim et al., 2015). Despite therapeutic potential and studies on the mode of action of the compound, the structure-function relationship (SAR) studies in the previous report were limited to a Michael acceptor.

In this study, based on a library of STAT3 inhibitors including a novel series of derivatives of the previously reported compound (compound 1; Fig. 1A), we intended to establish a detailed SAR between the Michael acceptor compounds and anticancer activities on retinoblastoma cell lines with activated STAT3. Then, we selected the two most potent STAT3 inhibitors and tested their effects on the phosphorylation of STAT3, the transcription activity of STAT3, and in vivo formation of retinoblastoma tumors in an orthotopic transplantation model. In addition, the potential toxicity of the STAT3 inhibitors was evaluated in vitro and in vivo.

Materials and Methods

Chemicals. We obtained all small molecular compounds to evaluate biologic activities from an in-house library of the Suh research laboratory.

2-(3,4-Dimethoxyphenyl)-1-(5-methoxy-2,2-dimethyl-2H-chromen-6-yl)prop-2-en-1-one (1). Detailed chemical spectral data are the same as compound **6** in the previous study (Kim et al., 2015).

2-(3,4-Dimethoxyphenyl)-1-(5-methoxy-2,2-dimethyl-2H-chromen-6-yl)prop-2-en-1-ol (2). Detailed chemical spectral data are the same as compound **21** in the previous study (Kim et al., 2015).

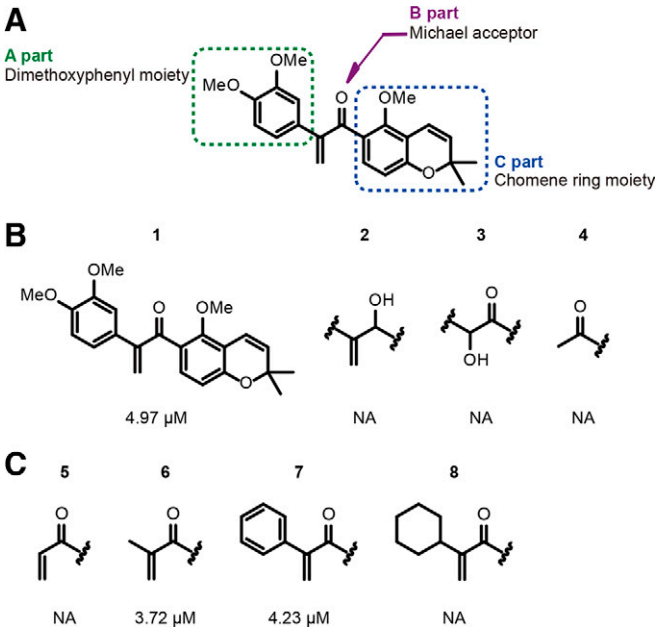

Fig. 1. Structures and structure-activity relationships of a library of STAT3 inhibitors regarding the Michael acceptor. (A) The structure of the parental compound, SH-48 (analog **1**), consisting of three parts: the A part with a dimethoxyphenyl moiety, the B part with a Michael acceptor, and the C part with a chromene ring moiety. (B) The GI_{50} values of analogs **1**–**4** with modification of a Michael acceptor moiety. (C) The GI_{50} values of analogs **5**–**8** with modification of the α-position of Michael acceptor. NA, not available.

2-(3,4-Dimethoxyphenyl)-2-hydroxy-1-(5-methoxy-2,2-dimethyl-2H-chromen-6-yl)ethan-1-one (3). 1 H NMR (800 MHz, CDCl3) δ 7.38 (d, J = 8.6 Hz, 1H), 6.82 (dd, J = 8.3, 2.1 Hz, 1H), 6.77 (d, J = 2.1 Hz, 1H), 6.71 (d, J = 8.2 Hz, 1H), 6.51 (dd, J = 11.3, 9.5 Hz, 2H), 5.93 (d, J = 5.3 Hz, 1H), 5.63 (d, J = 10.0 Hz, 1H), 4.56 (d, J = 6.3 Hz, 1H), 3.77 (d, J = 10.7 Hz, 6H), 3.67 (s, 3H), 1.39 (d, J = 4.0 Hz, 6H); ^{13}C NMR (200 MHz, CDCl3) δ 199.44, 158.44, 156.45, 148.96, 148.75, 131.60, 131.29, 130.66, 121.37, 119.76, 116.14, 114.78, 112.76, 111.01, 109.96, 77.14, 77.13, 63.22, 55.73, 55.72, 28.10, 28.06. high resolution mass spectrometry (HR-MS) (electrospray ionization (ESI)) calculated for $C_{22}H_{25}O_6$ (M + H+) 399.1808, found 399.1818.

1-(5-Methoxy-2,2-dimethyl-2H-chromen-6-yl)ethan-1-one (4). 1H NMR (800 MHz, chloroform-d (CDCl3)) δ 7.53 (d, J = 8.7 Hz, 1H), 6.58 (d, J = 8.7 Hz, 1H), 3.77 (s, 3H), 2.75 (t, J = 6.7 Hz, 2H), 2.58 (s, 3H), 1.79 (t, J = 6.7 Hz, 2H), 1.33 (s, 6H); 13C NMR (200 MHz, CDCl3) δ 198.44, 159.50, 159.03, 129.34, 123.93, 115.12, 113.38, 74.99, 61.63, 32.04, 29.99, 26.74, 17.26; HR-MS (ESI) calculated for $C_{14}H_{16}O_3$ (M) 232.1099, found 232.1110.

1-(5-Methoxy-2,2-dimethyl-2H-chromen-6-yl)prop-2-en-1-one (5). 1H NMR (800 MHz, CDCl3) δ 7.46 (d, J = 8.7 Hz, 1H), 7.10 (dd, J = 17.2, 10.4 Hz, 1H), 6.60 (d, J = 8.6 Hz, 1H), 6.33 (dd, J = 17.2, 1.7 Hz, 1H), 5.77 (dd, J = 10.4, 1.7 Hz, 1H), 3.71 (s, 3H), 2.74 (t, J = 6.8 Hz, 2H), 1.79 (t, J = 6.8 Hz, 2H), 1.33 (s, 6H); 13C NMR (200 MHz, CDCl3) δ 191.52, 159.44, 158.88, 136.00, 129.62, 128.20, 123.49, 115.03, 113.38, 75.00, 62.20, 32.02, 26.73, 17.15; HR-MS (ESI) calculated for $C_{15}H_{16}O_3$ (M) 244.1099, found 244.1109.

1-(5-Methoxy-2,2-dimethyl-2H-chromen-6-yl)-2-methylprop-2-en-1-one (6). 1H NMR (800 MHz, CDCl3) δ 7.08 (d, J = 8.4 Hz, 1H), 6.58 (d, J = 10.0 Hz, 1H), 6.54 (d, J = 8.3 Hz, 1H), 5.87 (m, 1H), 5.64 (m, 2H), 3.71 (s, 3H), 2.02 (s, 3H), 1.42 (s, 6H); 13C NMR (200 MHz, CDCl3) δ 197.65, 156.07, 154.92, 145.11, 130.54, 130.20, 128.16, 124.94, 116.62, 114.72, 111.49, 76.50, 63.04, 27.94, 17.68; HR-MS (ESI) calculated for $C_{16}H_{18}O_3$ (M) 258.1256, found 258.1266.

1-(5-methoxy-2,2-dimethyl-2H-chromen-6-yl)-2-phenylprop-2-en-1-one (7). 1H NMR (800 MHz, CDCl3) δ 7.42 (dd, J = 8.3, 1.2 Hz, 1H), 7.34 (dd, J = 16.4, 8.1 Hz, 2H), 7.30 (d, J = 7.3 Hz, 1H), 6.54 (m, 1H), 6.03 (s, 1H), 5.70 (s, 1H), 5.65 (d, J = 10.0 Hz, 1H), 3.75 (s, 2H), 1.43 (s, 3H); 13C NMR (200 MHz, CDCl3) δ 196.30, 157.33, 156.18, 149.86, 137.03, 131.69, 130.45, 128.35, 128.15, 127.60, 124.97, 123.48, 116.58, 114.87, 111.88, 76.79, 63.18, 28.03; HR-MS (ESI) calculated for $C_{21}H_{20}O_3$ (M) 320.1412, found 320.1421.

2-Cyclohexyl-1-(5-methoxy-2,2-dimethyl-2H-chromen-6-yl)prop-2-en-1-one (8). 1H NMR (800 MHz, CDCl3) δ 7.08 (d, J = 8.4 Hz, 1H), 6.58 (d, J = 10.0 Hz, 1H), 6.53 (d, J = 8.4 Hz, 1H), 5.71 (s, 1H), 5.64 (d, J = 10.0 Hz, 1H), 5.58 (s, 1H), 3.72 (s, 3H), 1.42 (s, 6H); 13C NMR (200 MHz, CDCl3) δ 197.77, 156.22, 155.20, 155.17, 130.66, 130.49, 125.65, 124.22, 116.67, 114.75, 111.48, 76.52, 63.06, 37.96, 32.34, 27.95, 26.59, 26.30; HR-MS (ESI) calculated for $C_{21}H_{26}O_3$ (M) 326.1882, found 326.1897.

2-(3,4-Dichlorophenyl)-1-(5-methoxy-2,2-dimethyl-2H-chromen-6-yl)prop-2-en-1-one (9). 1H NMR (800 MHz, CDCl3) δ 7.55 (d, J = 2.1 Hz, 1H), 7.40 (d, J = 8.3 Hz, 1H), 7.33 (d, J = 8.5 Hz, 1H), 7.26 (dd, J = 8.3, 2.1 Hz, 1H), 6.57 (dd, J = 17.5, 9.3 Hz, 2H), 6.03 (s, 1H), 5.75 (s, 1H), 5.66 (d, J = 10.0 Hz, 1H), 3.72 (s, 3H), 1.44 (s, 6H), 1.23 (s, 1H); 13C NMR (200 MHz, CDCl3) δ 195.35, 157.67, 156.19, 147.76, 136.98, 132.28, 131.47, 130.64, 130.26, 129.52, 127.02, 124.71, 116.42, 114.90, 112.13, 63.25, 28.06; HR-MS (ESI) calculated for $C_{21}H_{18}Cl_2O_3$ (M + H+) 389.0711, found 389.0722.

2-(3,4-Difluorophenyl)-1-(5-methoxy-2,2-dimethyl-2H-chromen-6-yl)prop-2-en-1-one (10). 1H NMR (800 MHz, CDCl3) δ 7.33 (d, J = 8.5 Hz, 1H), 7.29 (ddd, J = 11.4, 7.6, 2.1 Hz, 1H), 7.13 (m, 1H), 7.11 (dt, J = 9.8, 8.2 Hz, 1H), 6.57 (dd, J = 14.5, 9.2 Hz, 2H), 5.99 (s, 1H), 5.72 (s, 1H), 5.66 (d, J = 10.0 Hz, 1H), 3.72 (s, 3H), 1.44 (s, 6H); 13C NMR (200 MHz, CDCl3) δ 195.57, 157.60, 156.15, 147.91, 131.45, 130.63, 124.63, 124.34, 123.89, 123.88, 123.86, 123.85, 117.15, 117.06, 116.83, 116.74, 116.42, 114.89, 112.09, 76.91, 63.23, 28.04; HR-MS (ESI) calculated for $C_{21}H_{18}F_2O_3$ (M) 356.1224, found 356.1227.

2-(4-Fluoro-3-(trifluoromethyl)phenyl)-1-(5-methoxy-2,2-dimethyl-2H-chromen-6-yl)prop-2-en-1-one (11). 1H NMR (800 MHz, CDCl3) δ 7.68 (dd, J = 6.7, 2.1 Hz, 1H), 7.61 (ddd, J = 8.0, 4.6, 2.3 Hz, 1H), 7.32 (d, J = 8.5 Hz, 1H), 7.15 (m, 1H), 6.55 (m, 2H), 6.06 (s, 1H), 5.80 (s, 1H), 5.67 (d, J = 10.0 Hz, 1H), 3.73 (s, 3H), 1.44 (s, 6H); 13C NMR (200 MHz, CDCl3) δ 195.45, 157.59, 156.06, 147.56, 133.46, 133.44, 133.33, 133.29, 131.27, 130.71, 126.56, 126.54, 125.54, 124.53, 116.87, 116.76, 116.38, 114.91, 112.12, 76.91, 63.24, 28.01, 27.99; HR-MS (ESI) calculated for $C_{22}H_{18}F_4O_3$ (M) 406.1192, found 406.1192.

1-(5-Methoxy-2,2-dimethyl-2H-chromen-6-yl)-2-(4-methoxyphenyl)prop-2-en-1-one (12). 1H NMR (800 MHz, CDCl3) δ 7.36 (m, 1H), 7.34 (d, J = 8.5 Hz, 1H), 6.85 (m, 1H), 6.57 (m, 1H), 6.55 (dd, J = 8.5, 0.5 Hz, 1H), 5.95 (s, 1H), 5.64 (d, J = 10.0 Hz, 1H), 5.59 (s, 1H), 3.79 (s, 2H), 3.75 (s, 2H), 1.43 (s, 3H); 13C NMR (200 MHz, CDCl3) δ 196.66, 159.60, 157.28, 156.18, 149.24, 131.72, 130.42, 129.50, 128.81, 125.07, 121.80, 116.61, 114.86, 113.79, 111.84, 76.78, 63.17, 55.28, 28.03; HR-MS (ESI) calculated for $C_{22}H_{22}O_4$ (M) 350.1518, found 350.1519.

2-(4-Hydroxyphenyl)-1-(5-methoxy-2,2-dimethyl-2H-chromen-6-yl)prop-2-en-1-one (13). 1H NMR (800 MHz, CDCl3) δ 7.34 (d, *J* = 8.5 Hz, 1H), 7.32 (d, *J* = 8.7 Hz, 2H), 6.79 (d, *J* = 8.7 Hz, 1H), 6.62–6.51 (m, 2H), 5.95 (s, 1H), 5.65 (d, *J* = 10.0 Hz, 1H), 5.60 (s, 1H), 3.74 (s, 3H), 1.43 (s, 8H); 13C NMR (200 MHz, CDCl3) δ 196.65, 157.32, 156.18, 155.62, 149.17, 131.71, 130.46, 129.76, 129.39, 129.09, 121.99, 116.60, 115.25, 114.87, 114.46, 111.86, 63.19, 28.04; HR-MS (ESI) calculated for $C_{21}H_{21}O_4$ (M + H+) 337.1440, found 337.1457.

2-(4-Chlorophenyl)-1-(5-methoxy-2,2-dimethyl-2H-chromen-6-yl)prop-2-en-1-one (14). 1H NMR (800 MHz, CDCl3) δ 7.35 (m, 1H), 7.33 (d, J = 8.5 Hz, 1H), 7.29 (m, 1H), 6.55 (m, 1H), 6.01 (s, 1H), 5.71 (s, 1H), 5.65 (d, J = 10.0 Hz, 1H), 3.73 (s, 1H), 1.43 (s, 3H); 13C NMR (200 MHz, CDCl3) δ 195.91, 157.50, 156.16, 148.78, 135.47, 134.14, 131.54, 130.55, 128.94, 128.54, 124.76, 123.81, 116.48, 114.88, 112.02, 63.22, 28.04; HR-MS (ESI) calculated for $C_{21}H_{19}ClO_3$ (M) 354.1023, found 354.1024.

2-(2-Chlorophenyl)-1-(5-methoxy-2,2-dimethyl-2H-chromen-6-yl)prop-2-en-1-one (15). 1H NMR (800 MHz, CDCl3) δ 7.43 (d, J = 8.4 Hz, 1H), 7.36 (dd, J = 3.9, 2.3 Hz, 1H), 7.30 (m, 1H), 7.26 (m, 2H), 6.55 (m, 2H), 6.04 (dd, J = 33.9, 0.6 Hz, 2H), 5.66 (d, J = 10.0 Hz, 1H), 3.81 (s, 3H), 1.43 (s, 6H); 13C NMR (200 MHz, CDCl3) δ 194.25, 156.83, 155.95, 148.80, 137.21, 132.90, 131.61, 131.45, 130.50, 130.05, 129.45, 129.39, 126.79, 124.54, 116.60, 115.13, 111.46, 76.68, 63.48, 28.00; HR-MS (ESI) calculated for $C_{21}H_{19}ClO_3$ (M) 354.1023, found 354.1025.

2-(4-Fluorophenyl)-1-(5-methoxy-2,2-dimethyl-2H-chromen-6-yl)prop-2-en-1-one (16). 1H NMR (800 MHz, CDCl3) δ 7.38 (m, 1H), 7.33 (d, J = 8.5 Hz, 1H), 7.00 (m, 1H), 6.57 (d, J = 1.7 Hz, 1H), 5.99 (s, 1H), 5.69 (s, 1H), 5.65 (d, J = 10.0 Hz, 1H), 3.74 (s, 2H), 1.43 (s, 3H); 13C NMR (200 MHz, CDCl3) δ 196.16, 163.32, 162.09, 157.40, 156.11, 148.79, 133.10, 133.08, 131.51, 130.54, 129.44, 129.40, 124.88, 123.67, 116.51, 115.33, 115.23, 114.88, 111.96, 63.22, 28.03, 27.70; HR-MS (ESI) calculated for $C_{21}H_{19}FO_3$ (M) 338.1318, found 338.1328.

2-(3-Fluorophenyl)-1-(5-methoxy-2,2-dimethyl-2H-chromen-6-yl)prop-2-en-1-one (17). 1H NMR (800 MHz, CDCl3) δ 7.35 (d, J = 8.5 Hz, 1H), 7.29 (td, J = 8.0, 6.0 Hz, 1H), 7.18 (m, 1H), 7.15 (m, 1H), 6.99 (m, 1H), 6.57 (d, J = 1.7 Hz, 1H), 6.56 (d, J = 3.4 Hz, 1H), 6.03 (s, 1H), 5.73 (s, 1H), 5.65 (d, J = 10.0 Hz, 1H), 3.74 (s, 2H), 1.43 (s, 6H); 13C NMR (201 MHz, CDCl3) δ 195.71, 157.54, 156.23, 148.80, 148.79, 139.15, 139.11, 131.61, 130.55, 129.82, 129.78, 124.72, 124.17, 123.34, 123.32, 116.49, 115.09, 114.99, 114.89, 114.65, 114.54, 112.03, 63.21, 28.04; HR-MS (ESI) calculated for $C_{21}H_{19}FO_3$ (M) 338.1318, found 338.1323.

2-(2-Fluorophenyl)-1-(5-methoxy-2,2-dimethyl-2H-chromen-6-yl)prop-2-en-1-one (18). 1H NMR (800 MHz, CDCl3) δ 7.34 (d, J = 8.4 Hz, 1H), 7.27 (m, 2H), 7.12 (td, J = 7.5, 1.1 Hz, 1H), 7.04 (ddd, J = 10.0, 8.2, 0.9 Hz, 1H), 6.58 (d, J = 10.0 Hz, 1H), 6.56 (dd, J = 8.4, 0.5 Hz, 1H), 6.10 (s, 1H), 5.96 (s, 1H), 5.65 (d, J = 10.0 Hz, 1H), 3.78 (s, 3H), 1.43 (s, 6H); 13C NMR (201 MHz, CDCl3) δ 194.77, 160.42, 159.19, 157.09, 155.98, 145.23, 131.58, 130.73, 130.72, 130.47, 130.00, 129.96, 128.22, 125.69, 125.61, 124.45, 124.10, 124.08, 116.59, 115.68, 115.57, 114.93, 111.81, 76.74, 63.25, 28.02; HR-MS (ESI) calculated for $C_{21}H_{19}FO_3$ (M) 338.1318, found 338.1313.

1-(5-Methoxy-2,2-dimethyl-2H-chromen-6-yl)-2-(4-(trifluoromethyl)phenyl)prop-2-en-1-one (19). 1H NMR (800 MHz, CDCl3) δ 7.57 (dd, J = 45.5, 8.2 Hz, 4H), 7.35 (d, J = 8.5 Hz, 1H), 6.57 (m, 1H), 6.56 (d, J = 10.0 Hz, 1H), 6.08 (s, 1H), 5.81 (s, 1H), 5.66 (d, J = 10.0 Hz, 1H), 3.73 (s, 3H), 1.44 (s, 6H), 1.23 (s, 2H); 13C NMR (201 MHz, CDCl3) δ 195.56, 157.61, 156.17, 148.77, 140.58, 131.47, 130.63, 127.99, 125.31, 125.29, 125.21, 124.62, 116.43, 114.91, 112.12, 76.91, 63.24, 29.69, 28.04; HR-MS (ESI) calculated for $C_{22}H_{19}F_3O_3$ (M) 388.1286, found 388.1291.

1-(5-Methoxy-2,2-dimethyl-2H-chromen-6-yl)-2-(3-(trifluoromethyl)phenyl)prop-2-en-1-one (20). 1H NMR (800 MHz, CDCl3) δ 7.70 (s, 1H), 7.61 (d, J = 7.8 Hz, 1H), 7.57 (d, J = 7.8 Hz, 1H), 7.46 (t, J = 7.7 Hz, 1H), 7.35 (d, J = 8.5 Hz, 1H), 6.58 (m, 1H), 6.56 (d, J = 10.0 Hz, 1H), 6.10 (s, 1H), 5.81 (s, 1H), 5.66 (d, J = 10.0 Hz, 1H), 3.73 (s, 3H), 1.44 (s, 6H); 13C NMR (201 MHz, CDCl3) δ 195.61, 157.55, 156.14, 148.58, 137.81, 131.43, 131.10, 130.62, 128.76, 125.28, 116.45, 114.90, 112.06, 76.88, 63.23, 28.02; HR-MS (ESI) calculated for $C_{22}H_{19}F_3O_3$ (M) 388.1286, found 388.1292.

1-(5-Methoxy-2,2-dimethyl-2H-chromen-6-yl)-2-(2-(trifluoromethyl)phenyl)prop-2-en-1-one (21). 1H NMR (800 MHz, CDCl3) δ 7.69 (d, J = 7.9 Hz, 1H), 7.55 (t, J = 7.5 Hz, 1H), 7.45 (t, J = 7.7 Hz, 1H), 7.31 (d, J = 7.6 Hz, 1H), 7.28 (d, J = 8.3 Hz, 1H), 6.60 (t, J = 9.2 Hz, 2H), 6.10 (d, J = 12.3 Hz, 2H), 5.67 (d, J = 9.9 Hz, 1H), 3.80 (s, 3H), 1.44 (s, 6H); 13C NMR (201 MHz, CDCl3) δ 194.44, 156.49, 155.57, 147.82, 132.11, 132.06, 131.43, 130.66, 130.60, 128.02, 124.30, 116.61, 115.24, 111.54, 76.61, 63.47, 27.97; HR-MS (ESI) calculated for $C_{22}H_{19}F_3O_3$ (M) 388.1286, found 388.1299.

2-(3,5-Bis(trifluoromethyl)phenyl)-1-(5-methoxy-2,2-dimethyl-2H-chromen-6-yl)prop-2-en-1-one (22). 1H NMR (800 MHz, CDCl3) δ 8.17 (s, 2H), 7.89 (s, 1H), 7.86 (s, 1H), 7.82 (s, 1H), 7.47 (s, 1H), 7.34 (d, J = 8.5 Hz, 1H), 7.31 (s, 2H), 6.89 (d, J = 8.5 Hz, 1H), 6.61 (d, J = 8.4 Hz, 1H), 6.55 (d, J = 9.9 Hz, 1H), 6.45 (t, J = 8.9 Hz, 2H), 6.36 (d, J = 10.0 Hz, 1H), 6.21 (d, J = 8.3 Hz, 1H), 6.17 (s, 1H), 5.92 (s, 1H), 5.67 (d, J = 10.0 Hz, 1H), 5.65 (d, J = 10.0 Hz, 1H), 5.51 (d, J = 10.0 Hz, 1H), 3.72 (s, 3H), 3.65 (s, 3H), 3.45 (s, 3H), 3.08 (s, 1H), 2.63 (ddd, J = 17.5, 11.1, 6.5 Hz, 1H), 2.60 (s, 3H), 2.50 (d, J = 13.4 Hz, 1H), 2.05 (s, 1H), 1.44 (s, 6H), 1.44 (s, 3H), 1.40 (s, 3H), 1.37 (s, 3H), 1.27 (s, 3H), 1.23 (s, 3H); 13C NMR (200 MHz, CDCl3) δ 197.81, 157.37, 154.78, 131.27, 131.00, 130.81, 130.77, 130.08, 129.45, 128.22, 128.02, 127.05, 124.29, 116.84, 116.34, 116.17, 115.28, 114.57, 112.26, 111.99, 86.18, 63.30, 63.14, 61.75, 41.03, 28.06, 28.04, 27.67, 27.17; HR-MS (ESI) calculated for $C_{23}H_{18}F_6O_3$ (M) 456.1160, found 456.1181.

4-(3-(5-Methoxy-2,2-dimethyl-2H-chromen-6-yl)-3-oxoprop-1-en-2-yl)benzonitrile (23). ^{1}H NMR (800 MHz, CDCl3) δ 7.63 (d, *J* = 8.3 Hz, 1H), 7.53 (d, *J* = 8.3 Hz, 1H), 7.35 (d, *J* = 8.4 Hz, 1H), 6.58 (d, *J* = 8.5 Hz, 1H), 6.54 (d, *J* = 9.9 Hz, 1H), 6.09 (s, 1H), 5.84 (s, 1H), 5.66 (d, *J* = 10.0 Hz, 1H), 3.71 (s, 2H), 1.44 (s, 4H); 13C NMR (200 MHz, CDCl3) δ 195.15, 157.83, 156.21, 148.51, 141.62, 132.90, 132.15, 131.46, 130.72, 128.32, 127.94, 125.57, 124.44, 118.74, 116.35, 114.92, 112.26, 111.77, 63.27, 28.07; HR-MS (ESI) calculated for $C_{22}H_{19}NO_3$ (M) 345.1373, found 345.1365.

3-(3-(5-Methoxy-2,2-dimethyl-2H-chromen-6-yl)-3-oxoprop-1-en-2-yl)benzonitrile (24). 1H NMR (800 MHz, CDCl3) δ 7.74 (t, J = 1.5 Hz, 1H), 7.65 (ddd, J = 7.9, 1.6, 1.2 Hz, 1H), 7.59 (dt, J = 7.7, 1.3 Hz, 1H), 7.44 (t, J = 7.7 Hz, 1H), 7.34 (d, J = 8.5 Hz, 1H), 6.59 (dd, J = 8.5, 0.4 Hz, 1H), 6.55 (d, J = 10.1 Hz, 1H), 6.07 (s, 1H), 5.83 (s, 1H), 5.67 (dd, J = 9.9, 2.6 Hz, 1H), 3.72 (s, 3H), 1.44 (s, 6H), 1.43 (s, 1H), 1.34 (d, J = 18.9 Hz, 1H); 13C NMR (201 MHz, CDCl3) δ 195.19, 157.70, 156.11, 147.92, 138.34, 132.13, 131.56, 131.36, 131.35, 130.71, 129.13, 125.73, 124.44, 118.65, 116.36, 114.91,

112.61, 112.21, 76.95, 63.28, 28.05, 28.02; HR-MS (ESI) calculated for $C_{22}H_{19}NO_3$ (M) 345.1365, found 345.1381.

2-(3,4-Dimethoxyphenyl)-1-(2,2-dimethyl-2H-chromen-6-yl) prop-2-en-1-one (25). 1H NMR (800 MHz, CDCl3) δ 7.70 (dd, J = 8.5, 2.1 Hz, 1H), 7.61 (d, J = 2.1 Hz, 1H), 6.97 (d, J = 2.1 Hz, 1H), 6.94 (dd, J = 8.3, 2.1 Hz, 1H), 6.79 (m, 1H), 6.74 (d, J = 8.4 Hz, 1H), 6.30 (d, J = 9.9 Hz, 1H), 5.88 (s, 1H), 5.61 (m, 1H), 5.43 (s, 1H), 3.93 (d, J = 2.5 Hz, 2H), 3.86 (s, 3H), 3.84 (s, 3H), 2.02 (s, 1H), 1.44 (d, J = 2.6 Hz, 3H), 1.43 (s, 6H); 13C NMR (201 MHz, CDCl3) δ 196.54, 157.76, 149.34, 148.90, 147.85, 132.25, 131.10, 129.89, 129.85, 128.58, 121.61, 120.60, 119.75, 117.12, 116.07, 111.06, 110.29, 109.66, 77.68, 60.39, 55.89, 29.68, 28.53, 28.45, 21.04, 14.18; HR-MS (ESI) calculated for $C_{22}H_{22}O_4$ (M) 350.1518, found 350.1509.

Cells. Retinoblastoma cells from SNUOT-Rb1 (Kim et al., 2007), Y79 (catalog number HTB-18, ATCC; Manassas, VA), and WERI-Rb1 cells (catalog number HTB-169; ATCC) were maintained in RPMI 1640 media supplemented with 10% FBS and 1% antibiotics (catalog number 15240112; Thermo, Waltham, MA). STAT3 luciferase reporter HeLa stable cell line (catalog number SL-0003; Signosis, Santa Clara, CA) were maintained in Dulbecco's modified Eagle's medium media supplemented with 10% FBS and 1% antibiotics. ARPE-19 cells (catalog number CRL-2302; ATCC) were maintained in Dulbecco's modified Eagle's medium/F-12 media supplemented with 10% FBS and 1% antibiotics. Human retinal microvascular endothelial cells (HRMECs; catalog number ACBRI 181; Cell Systems, Kirkland, WA) were maintained in Endothelial cell growth medium-2 media (catalog number CC-3162; Lonza, Basel, Switzerland).

Cell Viability Assay. SNUOT-Rb1, Y79, and WERI-Rb1 cells in growth media or serum-free media with 5 mg/ml human serum albumin on 96-well plates were treated with a library of STAT3 inhibitors at the concentrations of 100 nM to 10 μM for 48 hours. ARPE-19 cells and HRMECs in growth media on 96-well plates were treated with compound 11 or 15 at the concentrations of 1 and 10 μM for 48 hours. Then, the cell viability was assessed with the EZ-CYTOX kit (catalog number EZ-1000; DoGenBio, Seoul, Republic of Korea) according to the manufacturer's instructions. The concentrations at which a growth inhibition of 50% is achieved (GI_{50}) were the mean values of each GI_{50} of SNUOT-Rb1, Y79, and WERI-Rb1 cells.

Enzyme-Linked Immunosorbent Assay. Y79 cells on 24-well plates were treated with STAT3 inhibitors at the concentration of 1 μM for 30 minutes. Then, the cells were prepared for cell lysates with the cell lysis buffer (catalog number 9803; Cell Signaling Technology, Danvers, MA) containing protease and phosphatase inhibitor cocktails (catalog numbers P3100 and P3200, respectively; GenDEPOT, Barker, TX). The levels of phospho-STAT3 at the tyrosine residue 705 were measured using the PathScan Phospho-Stat3 (Tyr705) Sandwich ELISA Kit (catalog number 7300; Cell Signaling Technology) according to the manufacturer's instructions. Quantitative analyses were performed with $n = 4$ independent biologic replicates.

Luciferase Assay. STAT3 luciferase reporter HeLa stable cells with stable expression of a STAT3 luciferase reporter were treated with oncostatin M (10 ng/ml; catalog number 295-OM; R&D, Minneapolis, MN) without or with STAT3 inhibitors at the concentration of 1 μM for 24 hours. Then, the luciferase activity was measured using the Dual-Glo Luciferase Assay System (catalog number E2920; Promega, Madison, WI). Quantitative analyses were performed with $n = 4$ independent biologic replicates.

Western Blot. Equal amounts of extracted proteins (50 μg) from the cell lysates were separated by 7% SDS-PAGE and transferred to nitrocellulose membranes. Cell lysates were prepared from SNUOT-Rb1, Y79, and WERI-Rb1 cells under normal culture condition or Y79 cells after the treatment of compound 11 or 15 at the concentrations of 200 nM, 1 μM, and 10 μM for 12 hours. The membranes were incubated with primary antibodies to phospho-STAT3 at the tyrosine residue 705 (catalog number 9138; Cell Signaling Technology), STAT3 (catalog number 9139; Cell Signaling Technology), or β-actin (catalog number A2066; Sigma, St. Louis, MO) at 4°C overnight. Then, they were treated with appropriate species-specific secondary antibodies (catalog number sc-2357 and sc-516102; Santa Cruz, Dallas, TX) at room temperature for 1 hour. Reagents from the EZ-Western Lumi pico kit (catalog number DG-WP100; DoGenBio) were applied to the membranes to visualize the bands in the Image-Quant LAS4000 system with the accompanying software program (GE, Chicago, IL).

Real-Time Polymerase Chain Reaction. Total RNA from cell lysates of Y79 cells after the treatment of compound 11 or 15 at the concentrations of 1 μM for 12 hours was isolated using TRI Reagent (Molecular Research Center, Cincinnati, OH). The quality of the extracted RNA was evaluated using the NanoDrop 2000 Spectrophotometer (Thermo). Then, cDNA was prepared with the High-Capacity RNA-to-cDNA Kit (catalog number 4387406; Thermo). Real-time polymerase chain reaction was performed with the StepOnePlus Real-Time PCR System (Thermo) using TaqMan Fast Advanced Master Mix (Life Technologies) with Gene Expression Assays (catalog number 4453320; Thermo). Specific assay identifiers for gene expression analysis were as follows: *18S*, Hs99999901_s1; *BCL2*, HS00608023_m1; *BCL2L1*, Hs00236329_m1; *BIRC5*, Hs04194392_s1; *CCND1*, Hs00765553_m1; *CDKN1A*, Hs00355782_m1; *GAPDH*, Hs999999905_m1; *GUSB*, Hs9999 9908_m1; *HPRT1*, Hs99999909_m1; *MMP1*, Hs00899658_m1; *MMP9*, Hs00234579_m1; *MYC*, Hs00153408_m1; *VEGFA*, Hs00900055 _m1). *18S*, *GAPDH*, *GUSB*, and *HPRT1* are genes for endogenous control. All procedures were performed following the minimum information for publication of quantitative real-time polymerase chain reaction experiments guidelines.

Mice. The 6-week-old male BALB/c nude (OrientBio, Seongnam-si, Republic of Korea) and C57BL/6 (Koatech, Pyeongtaek-si, Republic of Korea) mice were maintained in a specific pathogen-free facility under a 12-hour light/dark cycle. All experiments were done following the Association for Research in Vision and Ophthalmology statement for the use of animals in ophthalmic and vision research and approved by the Institutional Care and Use Committee of Seoul National University.

Orthotopic Transplantation of Retinoblastoma Cells. SNUOT-Rb1, Y79, and WERI-Rb1 cells (5×10^4 cells per eye) were injected into the vitreous cavity of BALB/c nude mice. At 2 weeks later, PBS (1 μl) or STAT3 inhibitors (compound 11 or 15; at the concentration of 1 μM in 1 μl PBS) were injected into the vitreous cavity after the confirmation of intraocular tumor formation ($n = 10$). At 4 and 6 weeks after the primary injection of retinoblastoma cells (2 and 4 weeks after the injection of STAT3 inhibitors), the tumor formation was evaluated according to the previously reported visual grading system, from grade 0 to grade 5 (Jo et al., 2017). Then, the eyes were prepared for histologic evaluation with H&E staining.

Histologic and Terminal Deoxynucleotidyl Transferase dUTP Nick-End Labeling Analyses. C57BL/6 mice were treated with PBS (1 μl) or STAT3 inhibitors (compound 11 or 15; at the concentration of 1 μM in 1 μl PBS) via intravitreal administration ($n = 6$). At 7 days after the injection, the enucleated eyes were prepared for H&E staining and TUNEL. H&E-stained slides were evaluated to measure the ratio of the retinal thickness from the internal limiting membrane to the inner nuclear layer (A in the graph) to that from the internal limiting membrane to the outer nuclear layer (B in the graph). The mean numbers of TUNEL-positive cells were evaluated in 10 randomly selected fields in each slide at $\times$400 magnification.

Optomotor Response Measurement. A virtual-reality optokinetic system (OptoMotry HD, CerebralMechanics, Medicine Hat, Canada) was used to measure optomotor response in the form of grating acuity visual threshold, according to the manufacturer's instructions and previously reported publications (Prusky et al., 2004; Douglas et al., 2005). Briefly, mice ($n = 6$) were positioned on the center of the platform where they were exposed to a virtual rotating cylinder on 4 monitors around them. Visual thresholds were determined to produce the maximum spatial frequency (cycles per degrees), which the mice could respond to the rotating stimuli.

Statistics. Statistical analyses were performed using the GraphPad Prism 9 program (GraphPad, San Diego, CA) and IBM SPSS Statistics 26 (IBM, Armonk, NY). Specific statistical methods were indicated in the figure legends.

Results

SAR. We analyzed that the structure of **1** has three parts (Fig. 1A), a dimethoxyphenyl moiety (A part), a Michael acceptor (B part), and a chromene ring moiety (C part). We previously reported **1** containing Michael acceptor as a STAT3 inhibitor based on a luciferase reporter assay and cytotoxicity evaluation with several breast cancer cell lines (Kim et al., 2015). Through the previous study, we investigated several analogs without Michael acceptors and elucidated that the Michael acceptor is a crucial moiety for STAT3 inhibitory activity (Kim et al., 2015). Nonetheless, the earlier study has a limitation in terms of the structural diversity. Particularly, the detailed SAR studies of the substituent effect of the α-position of the Michael acceptor, the 3,4-methoxy benzene in the A part, were not included.

First, in this study, we investigated the role of a Michael acceptor in antiproliferative activities in three different retinoblastoma cell lines, SNUOT-Rb1, Y79, and WERI-Rb1 cells (Fig. 1, B and C). The parental compound 1 possessing 3,4-dimethoxybenzene group on the α-position of the Michael acceptor exhibited antiretinoblastoma activity with an average GI_{50} value of 4.97 μM. On the other hand, the alcohol analog 2, which was previously reported by our group (Kim et al., 2015), another alcohol analog, 3, of which *exo*-olefin of Michael acceptor was alternated to a hydroxyl group, and a simple ketone analog, 4, without Michael acceptor showed remarkably low antitumor activities (Fig. 1B). Surprisingly, the analog 5 without a substituent on the α-position of Michael acceptor also exhibited no antiretinoblastoma activity, although it possessed the Michael acceptor moiety (Fig. 1C). However, antiretinoblastoma activity was restored by introducing a simple methyl group (analog 6) on the α-position of the Michael acceptor (average GI_{50} of 3.72 μM; Fig. 1C). The analog 7 possessing a simple benzene group on the α-position of the Michael acceptor also showed good antiretinoblastoma activity (average GI_{50} of 4.23 μM), whereas the analog 8 possessing a cyclohexane on the α-position of the Michael acceptor had no activity (Fig. 1C). It is possible to suggest the size limit of the binding pocket on the α-position of the Michael acceptor based on the comparison among analogs 6, 7, and 8, because the methyl group and benzene group is small, flat, and planar compared with the cyclohexane group in terms of the three-dimensional conformation.

We next examined the effects of the A part variation on the antiretinoblastoma activity to investigate the substituent effect of the benzene ring (Fig. 2). We first evaluated simple benzene (analog **7**, average GI_{50} of 4.23 μM), 3,4-di-chloro, and 3,4-di-fluoro benzene (analog 9, average GI_{50} of 8.47 μM; and 10, average GI_{50} of 4.81 μM) analogs to examine the

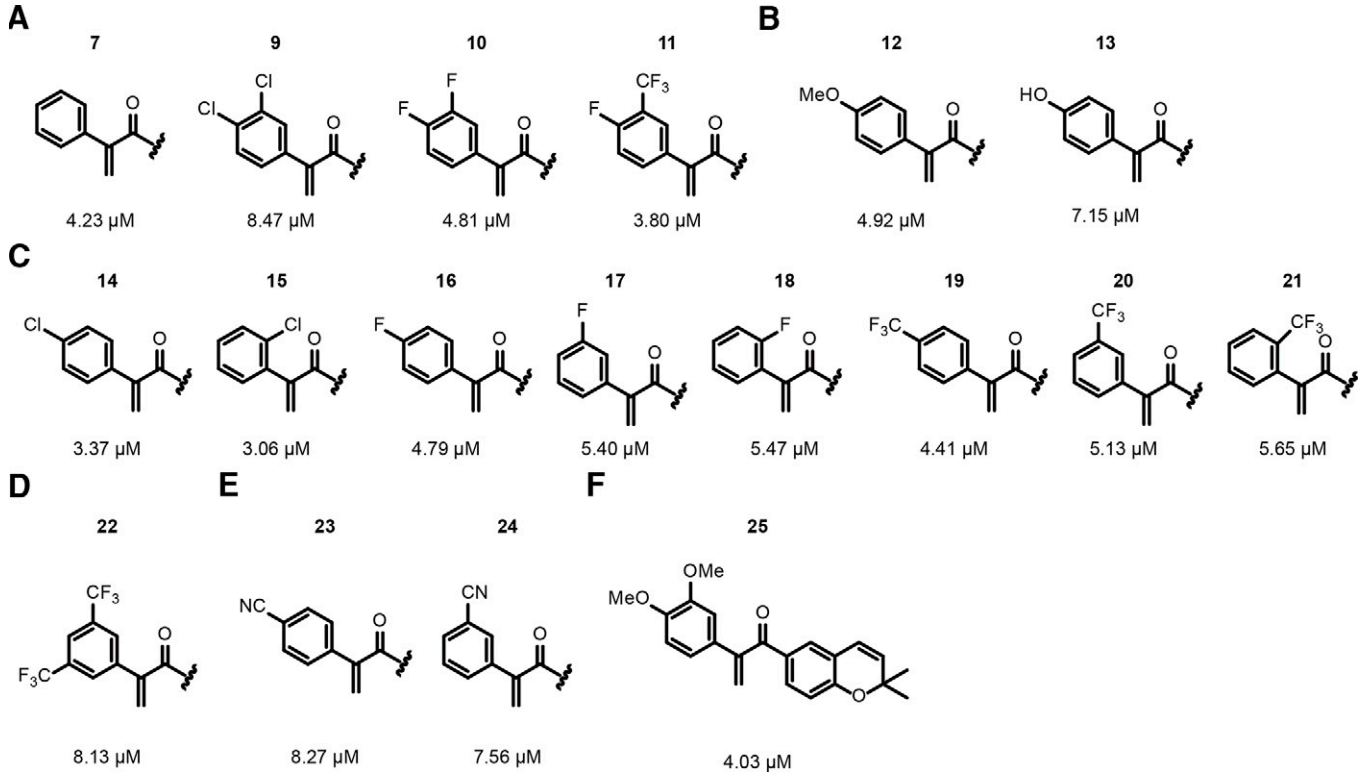

Fig. 2. Structures and structure-activity relationships of a library of STAT3 inhibitors regarding the dimethoxyphenyl and chromene ring moieties. (A–E) The GI_{50} values of analogs with modification of the A part. (A) Analogs with a simple benzene (analog **7**), 3,4-di-chloro (analog **9**) and 3,4-di-fluoro benzene (analog **10**), and 4-fluoro and 3-trifluoro benzene (analog 11) instead of the 3,4-dimethoxy benzene in the A part. (B) The monosubstituted methoxy analog (analog 12) and the demethylated analog 12 with hydroxyl analog (analog 13). (C) The analogs with the monoelectro withdrawing group substituted to chloro (analogs 14 and 15), fluoro (analogs 16–18), and trifluoro analogs (analogs 19–21). (D) The *meta,-meta*-di-trifluoro analog (analog 22). (E) The monocyano analogs (analogs 23 and 24). (F) The GI_{50} values of the demethoxy analog of the C part (a benzopyran moiety).

function of the 3,4-dimethoxy in the A part benzene ring (Fig. 2A). Although there has been controversy over the fluorine atom as a hydrogen bond acceptor in the benzene ring, a difluoro analog 10 exhibited potent activity compared with a dichloro analog 9 (Dunitz and Taylor, 1997; Bissantz et al., 2010). Interestingly, analog 11 containing 4-fluoro and 3-trifluoro as hybrid substituents of the benzene showed excellent cytotoxicity with an average GI_{50} value of 3.80 μM (Fig. 2A). These results implied the necessity of robust research on the substituent effect of the A part on antiretinoblastoma activity. The monosubstituted methoxy analog 12 (average GI_{50} of 4.92 μM) exhibited good cytotoxicity comparable to the parental compound 1. In contrast, the demethylated analog of 12, the hydroxyl analog 13 (average GI_{50} of 7.15 μM), which is a hydrogen bond donor, showed lower activity (Fig. 2B). The monoelectron withdrawing group-substituted chloro analogs (analog 14, average GI_{50} of 3.37 μM; and 15, average GI_{50} of 3.06 μM), fluoro analogs (analog 16, average GI_{50} of 4.7 μM; 17, average GI_{50} of 5.40 μM; and 18, average GI_{50} of 5.47 μM), and trifluoro analogs (analog 19, average GI_{50} of 4.41 μM; 20, average GI_{50} of 5.13 μM; and 21, average GI_{50} of 5.65 μM) showed excellent to good antiproliferative activities compared with the parental compound 1 (Fig. 2C). Remarkably, the *meta,meta*-di-trifluoro analog 22 (average GI_{50} of 8.13 μM) showed lower activity than the *meta*-mono-trifluoro analog 20 (Fig. 2D). It implied that the *meta*-mono trifluoro benzene might not be rotatable in the binding site. If it is rotatable in the binding site, the conformation and mode of action were very similar between *meta*-mono and *meta,meta*-di trifluoro benzenes. Analogs that have a monocyano group (analog 23, average GI_{50} of 8.27 μM; and 24, average GI_{50} of 7.56 μM) less hydrophobic than other electron-withdrawing groups exhibited lower activities (Fig. 2E).

Next, we investigated the role of a methoxy group at the 2-position in the C part carboxychromene moiety via comparing the parental compound 1 and the demethoxy analog 25 (average GI_{50} of 4.03 μM; Fig. 2F). The methoxy effect on the chromene ring did not play any significant role in the antiproliferative activity, which suggests the possibility of a tuning substituent of the chromene ring. The GI_{50} values showed similar patterns in all 3 tested cell lines, SNUOT-Rb1, Y79, and WERI-Rb1 (Table 1). Also, there were no definite differences in the GI_{50} values of analogs 11 and 15 in the experiments using 5 mg/ml of human serum albumin instead of 20% FBS to investigate whether there would be a shift of the values (3.72 μM versus 3.80 μM in analog 11 and 3.10 μM versus 3.06 μM in analog 15).

TABLE 1
GI_{50} values (μM) of each compound in SNUOT-Rb1, Y79, and WERI-Rb1 cells

	SNUOT-Rb1	Y79	WERI-Rb1	Average
1	4.95	5.13	4.82	4.97
2	NA	NA	NA	NA
3	NA	NA	NA	NA
4	NA	NA	NA	NA
5	NA	NA	NA	NA
6	3.63	3.58	3.95	3.72
7	4.09	4.37	4.24	4.23
8	NA	NA	NA	NA
9	8.10	9.18	8.13	8.47
10	4.24	5.45	4.75	4.81
11	2.96	4.77	3.66	3.80
12	5.04	5.18	4.53	4.92
13	5.98	7.81	7.65	7.15
14	2.62	3.66	3.84	3.37
15	1.98	3.39	3.81	3.06
16	4.31	5.54	4.53	4.79
17	4.86	6.39	4.97	5.40
18	4.45	6.65	5.29	5.47
19	4.90	4.27	4.07	4.41
20	5.02	5.21	5.16	5.13
21	4.59	7.07	5.29	5.65
22	7.98	9.00	7.41	8.13
23	8.07	8.15	8.58	8.27
24	7.60	7.55	7.53	7.56
25	3.73	4.52	3.83	4.03

Effects of Analogs on the Phosphorylation and the Transcription Activity of STAT3. To figure out whether antiproliferative effects of analogs were related to their inhibitory effects of STAT3, we measured the levels of phospho-STAT3 at the tyrosine residue 705 in Y79 cells upon the treatment with each analog at the concentration of 1 μM (Fig. 3A). Interestingly, simple methyl (analog 6), 4-fluoro, and 3-trifluoro benzene (analog 11), and monochloro benzene (analog 14 and 15) analogs exhibited better inhibitory effects on the phosphorylation of STAT3 than the parental compound 1 (Fig. 3A). In line with these results, these analogs also effectively suppressed the oncostatin M–induced transcription activity of STAT3 in cells from the HeLa stable cell

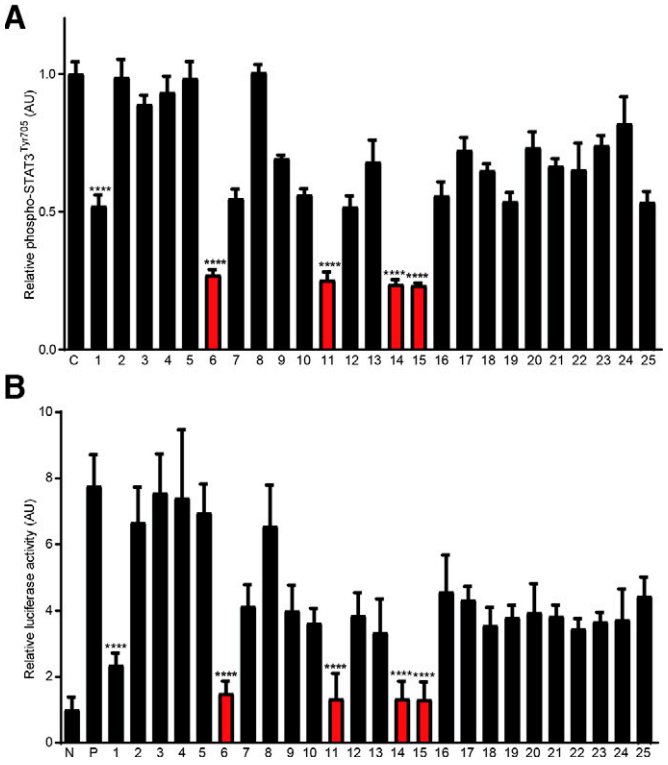

Fig. 3. Inhibition of phosphorylation and transcription activity of STAT3 by a library of STAT3 inhibitors. (A) The relative levels of phospho-STAT3 (Tyr705) in the cell lysates of Y79 cells after the treatment of a library of STAT3 inhibitors. (B) The relative levels of transcription activity of STAT3 on luciferase reporter assays. Mean ± S.D. of $n = 4$ independent biologic replicates. One-way ANOVA with post hoc Dunnett's multiple comparison tests. The value of each compound was compared with the values of the control group in Fig. 3A and the positive control group in Fig. 3B. ****$P < 0.0001$. Red dashed lines correspond to the values of the parental compound, analog 1. The analogs of which activities were better than the parental compound were indicated with the red bars. AU, artificial unit; C, control; N, negative control; P, positive control treated with oncostatin M.

line compared with the parental compound **1** at the concentration of 1 μM (Fig. 3B).

Inhibitory Effects of Analogs 11 and 15 on the Phosphorylation of STAT3 and the Transcription of STAT3-Related Genes. As in tumor tissues from patients with retinoblastoma and ?70% of solid cancers (Yu and Jove, 2004; Mohan et al., 2006; Jo et al., 2014), SNUOT-Rb1, Y79, and WERI-Rb1 cells showed the constituent activation of STAT3 under the normal culture condition (Fig. 4A). Analogs 11 and 15 effectively suppressed the phosphorylation of STAT3 in Y79 cells in a dose-dependent manner (Fig. 4, B–D). The target genes of STAT3 related to the tumorigenesis include *CCND1*, *CDKN1A* (cell cycle), *BCL2*, *BCL2L1*, *BIRC5*, *MYC* (antiapoptosis), *MMP1*, *MMP9* (migration, invasion), and *VEGFA* (angiogenesis) (Luwor et al., 2013). Analogs 11 and 15 significantly decreased the mRNA expression of the target genes of STAT3 in Y79 cells at the concentration of 1 μM (Fig. 4, E and F).

Suppression of In Vivo Formation of Retinoblastoma Tumors by Analogs 11 and 15. An orthotopic transplantation model is an effective tool to investigate the potential of therapeutic agents in the treatment of retinoblastoma (Jo et al., 2014; Jo et al., 2017). The visual grading system defines the intravitreal tumor from the grade 0 (no tumor), 1 (the streak-like tumor), 2 (the plaque-like tumor), 3 (evident mass formation), 4 (the vitreous-filling tumor), to 5 (the globe-enlarging tumor) (Jo et al., 2017). At 2 weeks after the intravitreal injection of retinoblastoma cells, we administered analogs 11 or 15 at the concentration of 1 μM in 1 μl PBS into the vitreous cavity. Then, at 4 weeks after the injection of tumor cells, the tumor formation was evaluated. In line with in vitro effects, the degrees of in vivo tumor formation were less severe in groups treated with analogs 11 or 15 compared with the control group treated with PBS ($P < 0.001$; Fig. 5A). There were no events of regrowth of tumors with additional 2-week follow-up. In contrast, the mice in the control groups failed to endure the additional follow-up period because of eyeball rupture due to tumor enlargement. H&E slides also showed that there were no definite tumor remnants in the vitreous cavity facing the retinal tissue in groups treated with analogs 11 or 15 (Fig. 5, B–D).

No Definite In Vitro and In Vivo Toxicities of Analog 11 and 15. In the treatment of pediatric cancers, one of the major concerns is systemic and local toxicity related to chemotherapy. ARPE-19 cells and HRMECs represent retinal pigment epithelial and microvascular endothelial cells, respectively. Interestingly, these cells did not express constitutive activation of STAT3 in normal culture conditions compared with retinoblastoma cells, SNUOT-Rb1, Y79, and WERI-Rb1 cells (Jo et al., 2014). Even at 10 μM, analogs 11 and 15 did not affect the cellular viability of ARPE-19 cells and HRMECs (Fig. 6, A and B). Also, these analogs did not induce the change in the histologic integrity (Fig. 6, C and

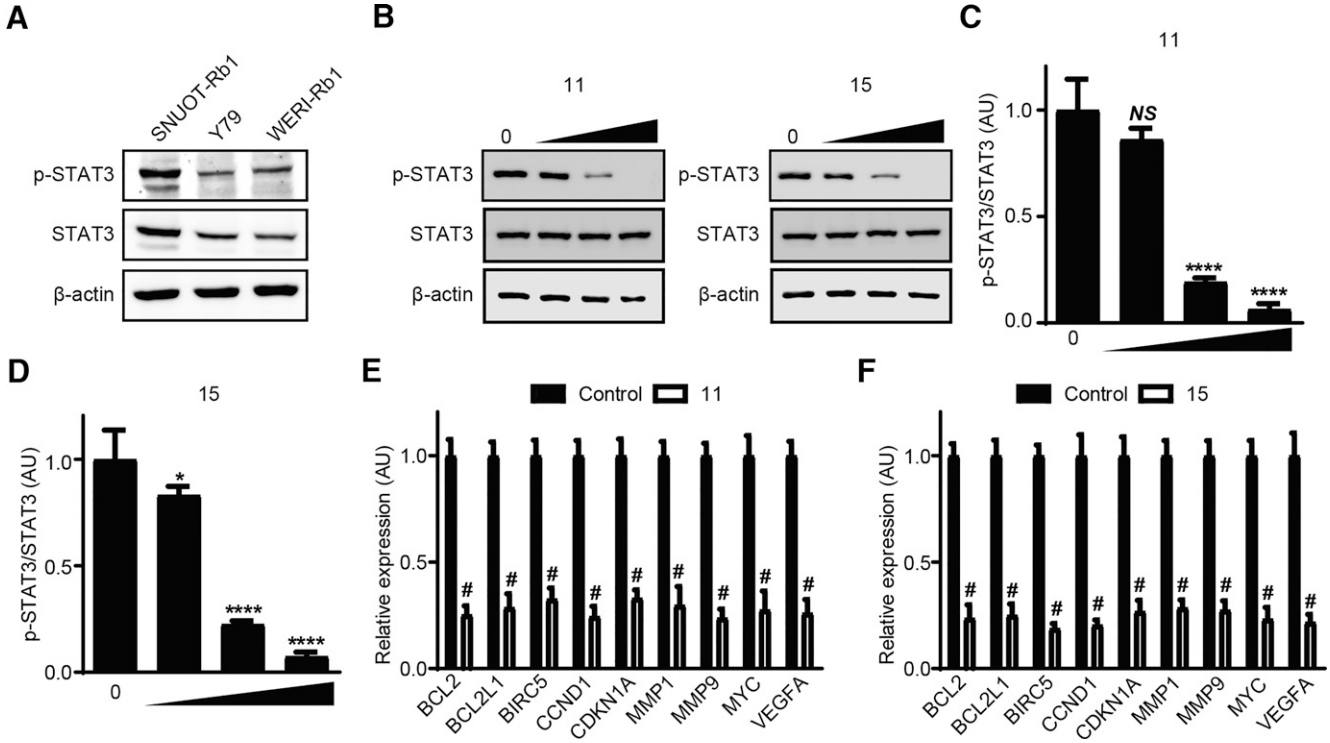

Fig. 4. Suppression of phosphorylation of STAT3 and expression of the target genes of STAT3 by analogs 11 and 15. (A) The protein expression of phospho-STAT3 (Tyr705) and STAT3 in SNUOT-Rb1, Y79, and WERI-Rb1 cells. (B) The protein expression of phospho-STAT3 (Tyr705) and STAT3 in Y79 cells after the treatment of analogs 11 and 15. (C and D) The relative values of the ratios of phospho-STAT3 to STAT3 upon treatment with analogs 11 (C) and 15 (D) at the concentrations of 200 nM, 1 μM, and 10 μM. Mean ± S.D. of $n = 4$ independent biologic replicates. The value of each treatment group was compared with the values of the control group. One-way ANOVA with Dunnett's multiple comparison tests. (E and F) The relative values of gene expression of target genes of STAT3 after the treatment of analogs 11 (E) and 15 (F). Mean ± S.D. of $n = 4$ independent biologic replicates. The value of each treatment group was compared with the values of the control group. Two-way ANOVA with post hoc Tukey's multiple comparison tests. *NS*, $P > 0.05$; $^{*}P < 0.05$; **** and $^{\#}P < 0.0001$. AU, artificial unit; p-STAT3, phospho-STAT3 at the Tyr705 residue.

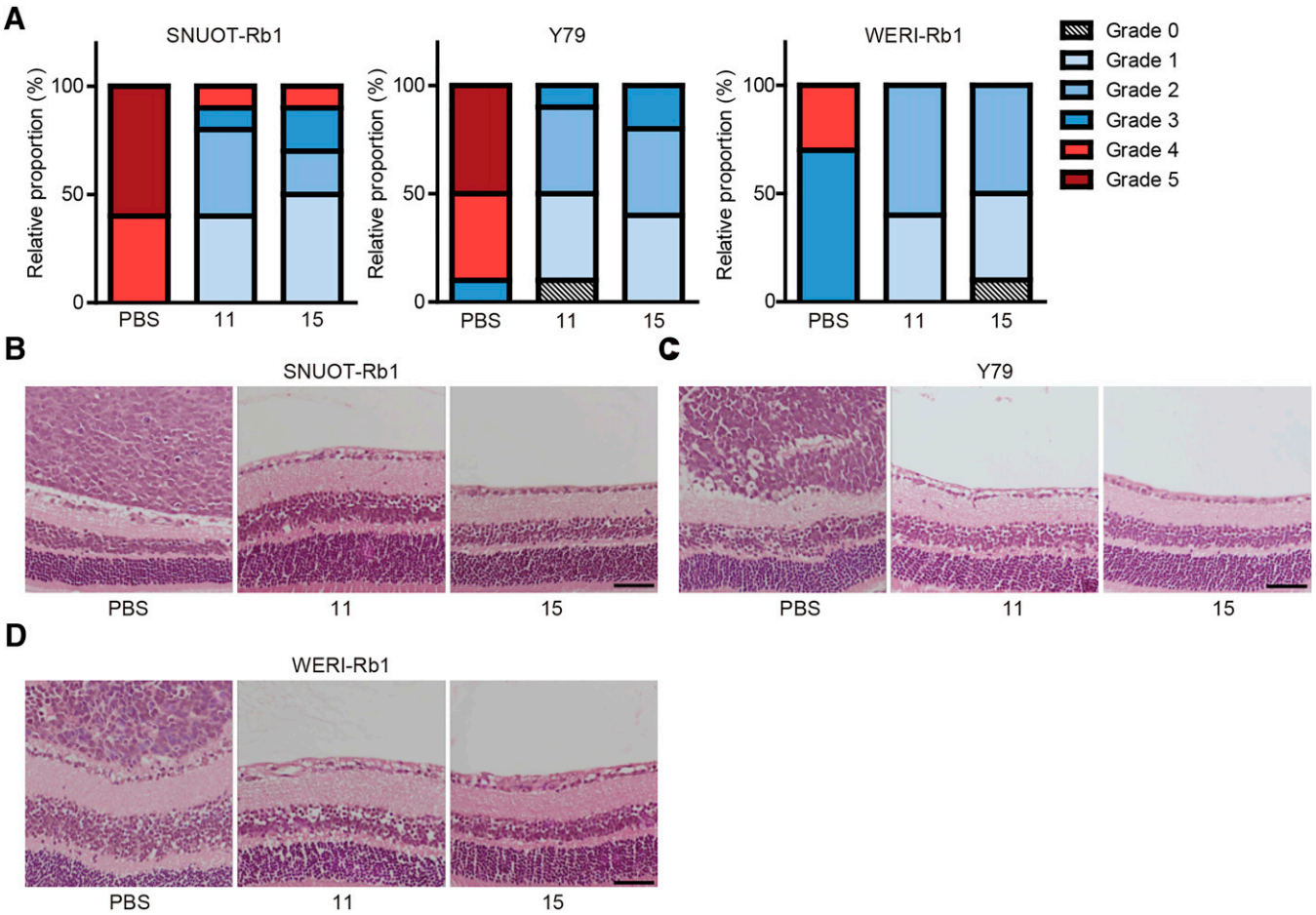

Fig. 5. In vivo inhibition of the formation of retinoblastoma tumors by analogs 11 and 15. (A) The proportions of grade 0–5 intraocular tumors in the eyes of male BALB/c nude mice (n = 10) at 1 month after the intravitreal injection of SNUOT-Rb1, Y79, and WERI-Rb1 cells. Analogs 11 and 15 were intravitreally injected at 2 weeks after the intravitreal injection of tumor cells. Grade 0, no evidence of tumor; grade 1, streak-like tumor; grade 2, plaque-like tumor; grade 3, definite mass; grade 4, vitreous-filling mass; grade 5, mass with globe enlargement or eyeball rupture. Fisher's exact tests showed that P values were less than 0.0001 in all 3 experiments. (B–D) The representative images of eyes of male BALB/c nude mice (n = 10) at 1 month after the intravitreal injection of SNUOT-Rb1, Y79, and WERI-Rb1 cells. Analogs 11 and 15 were injected at 2 weeks after the intravitreal injection of tumor cells. Scale bar, 50 μm.

D), the apoptotic activity (Fig. 6, E and F), the visual function (Fig. 6G), and body weight (Fig. 6H) at 1 week after they were administered into the vitreous cavity at the concentration of 10 μM, 10 times the therapeutic concentration.

Discussion

In this study, we established a detailed SAR between analogs from a library of derivatives of compound **1** and antitumor activities. We confirmed that the Michael acceptor was the key moiety in the inhibition of STAT3 activation in line with previous studies (Butturini et al., 2011, 2013; Don-Doncow et al., 2014; Kim et al., 2015). Furthermore, among the derivatives, we found that analogs 11 and 15 were the most potent in the inhibition of the phosphorylation and transcription activity of STAT3. These analogs effectively suppressed the phosphorylation of STAT3 at the tyrosine residue 705 of Y79 cells, which demonstrates the constitutive activation of STAT3. They also decreased the expression of the target genes of STAT3. These data implied that analogs 11 and 15 were STAT3 inhibitors as the parental compound 1. The in vivo experiments using an orthotopic transplantation model showed that these novel STAT3 inhibitors suppressed the tumor formation in the vitreous cavity. Despite their potent in vitro and in vivo effects, these analogs did not affect the cellular viability of retinal constituent cells and the histologic integrity of retinal tissues. Also, they did not induce changes in the visual threshold to rotating stimuli and body weight.

STAT3 inhibitors seem to have potential in cancer therapy in that STAT3 is persistently and constitutively activated in many malignancies, resulting in cell proliferation, survival, and angiogenesis (Wong et al., 2017). Canonical STAT3 activation by the phosphorylation at the tyrosine residue 705 leads to STAT3 dimerization, nuclear translocation, and binding to a canonical sequence of DNA (Huynh et al., 2019). Direct and indirect STAT3 inhibitors target STAT3 protein directly and upstream regulators of STAT3 pathway, respectively (Wong et al., 2017; Lee et al., 2019). Direct inhibitors usually block the SH2 domain for dimerization or the DNA-binding domain (Lee et al., 2019). The parental compound 1 of the derivatives in this study directly binds to STAT3, further disrupting the dimerization and translocation of STAT3 (Kim et al., 2015). In this context, we speculated that further studies with large animals might be necessary to figure out

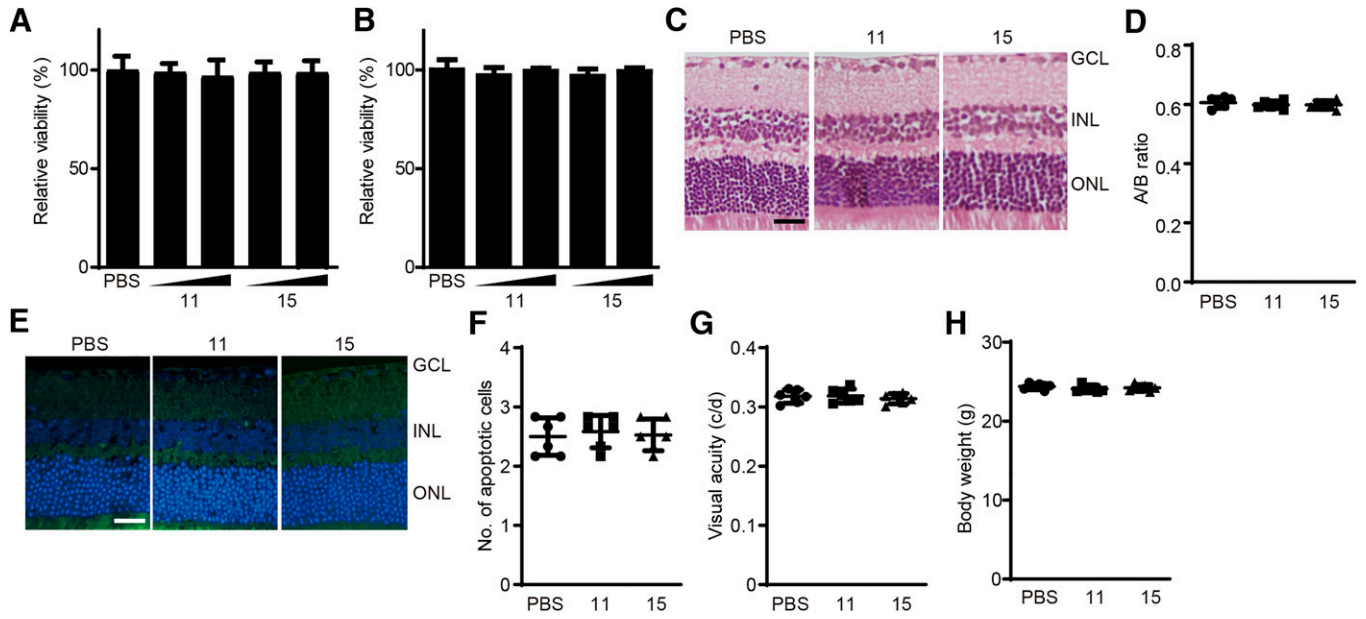

Fig. 6. In vitro and in vivo toxicity profiles of analogs 11 and 15. (A and B) The cellular viability of ARPE-19 (A) and HRMECs (B) after the treatment of analogs 11 and 15. The concentrations of analogs were 1 and 10 μM. (C) The representative images of H&E-stained retinal tissues at 1 week after the intravitreal injection of analogs 11 and 15 (10 μM). (D) The relative ratios of the retinal thickness from the internal limiting membrane to the inner nuclear layer, A, to that from the internal limiting membrane to the outer nuclear layer, B (n = 6). (E) The representative images of TUNEL-stained retinal tissues at 1 week after the intravitreal injection of analogs 11 and 15 (10 μM). (F) The number of TUNEL-positive cells in each slide at ×400 magnification (n = 6). (G and H) Optomotor response (G) and body weight (H) at 1 weeks after the intravitreal injection of analogs 11 and 15 (10 μM). Mean ± S.D. of n = 6 independent biologic replicates. One-way ANOVA analyses showed that P values were over 0.05. Scale bar, 50 μm. GCL, ganglion cell layer; INL, inner nuclear layer; ONL, outer nuclear layer.

whether there would be intercalation of constituent proteins in the vitreous cavity in the action of STAT3 inhibitors in the eyes. Nevertheless, it is remarkable that there were no definite differences in the GI_{50} values in cellular viability assays in cell culture with growth media with 10% FBS and serum-free media with 5 mg/ml human serum albumin. Galiellalactone, which is also a Michael acceptor, covalently binds to STAT3 and inhibits its binding to DNA (Don-Doncow et al., 2014). Another mechanism of Michael acceptors to inhibit STAT3 activation is direct interaction with glutathione, triggering *S*-glutathionylation of STAT3 (Butturini et al., 2011, 2013).

As in other cancers, STAT3 is activated in retinoblastoma tumors. The immunoreactivity to the phosphorylated STAT3 is evident in 19 out of 22 tumor samples from patients with invasive retinoblastoma (Mohan et al., 2006). Similarly, we previously reported that retinoblastoma tissues from six patients with advanced tumors demonstrated highly positive nuclear staining of phosphorylated forms of STAT3 at the tyrosine residue 705 and serine residue 727 (Jo et al., 2014). We speculated that direct targeting to STAT3 might be a plausible way to treat patients with retinoblastoma. Currently, the first-line systemic chemotherapy regimen for retinoblastoma is limited to conventional drugs including vincristine, etoposide, and carboplatin. There are no definite second-line options for retractable retinoblastoma tumors to conventional drugs. STAT3 inhibitors might have a role in the treatment of retinoblastoma in that STAT3 is activated in invasive and advanced tumors (Mohan et al., 2006; Jo et al., 2014). Furthermore, previous studies on targeting STAT3 or the STAT3 pathway in retinoblastoma have demonstrated promising in vitro and in vivo results. Small interfering RNA targeting to STAT3 inhibited proliferation, invasion, and migration of Y79 cells (Jo et al., 2014; Liang et al., 2018). Also, it suppressed in vivo formation of orthotopic tumors in the vitreous cavity (Jo et al., 2014). Studies on the roles of microRNAs and long noncoding RNAs showed that STAT3 is a key mediator of their action (Liu et al., 2016; Hu et al., 2018; Liu et al., 2018; Zhang et al., 2018; Sun et al., 2020). The current study also demonstrated that novel STAT3 inhibitors from the in-house library showed in vitro and in vivo efficacy on retinoblastoma.

Novel STAT3 inhibitors from the library of derivatives of compound 1 effectively suppressed in vivo tumor formation and did not affect the histologic integrity of the retinal tissues. These STAT3 inhibitors can be used in the treatment of retinoblastoma in coordination with currently available chemotherapeutic agents in that they target the retinoblastoma-relevant STAT3 signaling pathway.

Authorship Contributions

Participated in research design: Suh, J. H. Kim.
Conducted experiments: Jo, Lee, Bak, Cho.
Contributed new reagents or analytic tools: Han, K. Kim.
Performed data analysis: Jo, Lee, Cho.
Wrote or contributed to the writing of the manuscript: Jo, Lee, Suh, J. H. Kim.

References

Bissantz C, Kuhn B, and Stahl M (2010) A medicinal chemist's guide to molecular interactions. *J Med Chem* **53**:5061–5084.

Butturini E, Carcereri de Prati A, Chiavegato G, Rigo A, Cavalieri E, Darra E, and Mariotto S (2013) Mild oxidative stress induces S-glutathionylation of STAT3 and enhances chemosensitivity of tumoural cells to chemotherapeutic drugs. *Free Radic Biol Med* **65**:1322–1330.

Butturini E, Cavalieri E, de Prati AC, Darra E, Rigo A, Shoji K, Murayama N, Yamazaki H, Watanabe Y, Suzuki H, et al. (2011) Two naturally occurring terpenes, dehydrocostuslactone and costunolide, decrease intracellular GSH content and inhibit STAT3 activation. *PLoS One* **6**:e20174.

Dimaras H and Corson TW (2019) Retinoblastoma, the visible CNS tumor: A review. *J Neurosci Res* **97**:29–44.
Dimaras H, Corson TW, Cobrinik D, White A, Zhao J, Munier FL, Abramson DH, Shields CL, Chantada GL, Njuguna F, et al. (2015) Retinoblastoma. *Nat Rev Dis Primers* **1**:15021.
Don-Doncow N, Escobar Z, Johansson M, Kjellström S, Garcia V, Munoz E, Sterner O, Bjartell A, and Hellsten R (2014) Galiellalactone is a direct inhibitor of the transcription factor STAT3 in prostate cancer cells. *J Biol Chem* **289**:15969–15978.
Douglas RM, Alam NM, Silver BD, McGill TJ, Tschetter WW, and Prusky GT (2005) Independent visual threshold measurements in the two eyes of freely moving rats and mice using a virtual-reality optokinetic system. *Vis Neurosci* **22**:677–684.
Dunitz JD and Taylor R (1997) Organic Fluorine Hardly Ever Accepts Hydrogen Bonds. *Chemistry* **3**:89–98.
Hu C, Liu S, Han M, Wang Y, and Xu C (2018) Knockdown of lncRNA XIST inhibits retinoblastoma progression by modulating the miR-124/STAT3 axis. *Biomed Pharmacother* **107**:547–554.
Huynh J, Chand A, Gough D, and Ernst M (2019) Therapeutically exploiting STAT3 activity in cancer - using tissue repair as a road map. *Nat Rev Cancer* **19**:82–96.
Jo DH, Kim JH, Cho CS, Cho YL, Jun HO, Yu YS, Min JK, and Kim JH (2014) STAT3 inhibition suppresses proliferation of retinoblastoma through down-regulation of positive feedback loop of STAT3/miR-17-92 clusters. *Oncotarget* **5**:11513–11525.
Jo DH, Lee K, Kim JH, Jun HO, Kim Y, Cho YL, Yu YS, Min JK, and Kim JH (2017) L1 increases adhesion-mediated proliferation and chemoresistance of retinoblastoma. *Oncotarget* **8**:15441–15452.
Johnson DE, O'Keefe RA, and Grandis JR (2018) Targeting the IL-6/JAK/STAT3 signalling axis in cancer. *Nat Rev Clin Oncol* **15**:234–248.
Kim JH, Kim JH, Yu YS, Kim DH, Kim CJ, and Kim KW (2007) Establishment and characterization of a novel, spontaneously immortalized retinoblastoma cell line with adherent growth. *Int J Oncol* **31**:585–592.
Kim K, Kim SJ, Han YT, Hong SJ, An H, Chang DJ, Kim T, Lim B, Lee J, Surh YJ, et al. (2015) Identification of small molecule inhibitors of the STAT3 signaling pathway: Insights into their structural features and mode of action. *Bioorg Med Chem Lett* **25**:5444–5448.
Lee H, Jeong AJ, and Ye SK (2019) Highlighted STAT3 as a potential drug target for cancer therapy. *BMB Rep* **52**:415–423.
Liang H, Wang G, Liu Y, Zhao G, Du J, and Zhao X (2018) Targeting STAT3 induces apoptosis and suppresses cell growth and invasion by inactivation of Slug signaling in retinoblastoma. *Int J Clin Exp Pathol* **11**:342–350.
Liu S, Hu C, Wang Y, Shi G, Li Y, and Wu H (2016) miR-124 inhibits proliferation and invasion of human retinoblastoma cells by targeting STAT3. *Oncol Rep* **36**:2398–2404.
Liu S, Zhang X, Hu C, Wang Y, and Xu C (2018) miR-29a inhibits human retinoblastoma progression by targeting STAT3. *Oncol Rep* **39**:739–746.
Luwor RB, Stylli SS, and Kaye AH (2013) The role of Stat3 in glioblastoma multiforme. *J Clin Neurosci* **20**:907–911.
Mohan A, Mallikarjuna K, Venkatesan N, Abhyankar D, Parikh PM, and Krishnakumar S (2006) The study of c-Src kinase and pStat3 protein expression in retinoblastoma. *Exp Eye Res* **83**:736–740.
Prusky GT, Alam NM, Beekman S, and Douglas RM (2004) Rapid quantification of adult and developing mouse spatial vision using a virtual optomotor system. *Invest Ophthalmol Vis Sci* **45**:4611–4616.
Sun X, Shen H, Liu S, Gao J, and Zhang S (2020) Long noncoding RNA SNHG14 promotes the aggressiveness of retinoblastoma by sponging microRNA-124 and thereby upregulating STAT3. *Int J Mol Med* **45**:1685–1696.
Wong ALA, Hirpara JL, Pervaiz S, Eu JQ, Sethi G, and Goh BC (2017) Do STAT3 inhibitors have potential in the future for cancer therapy? *Expert Opin Investig Drugs* **26**:883–887.
Yu H and Jove R (2004) The STATs of cancer–new molecular targets come of age. *Nat Rev Cancer* **4**:97–105.
Yu H, Lee H, Herrmann A, Buettner R, and Jove R (2014) Revisiting STAT3 signalling in cancer: new and unexpected biological functions. *Nat Rev Cancer* **14**:736–746.
Zhang A, Shang W, Nie Q, Li T, and Li S (2018) Long non-coding RNA H19 suppresses retinoblastoma progression via counteracting miR-17-92 cluster. *J Cell Biochem* **119**:3497–3509.

Address correspondence to: Jeong Hun Kim, Fight against Angiogenesis-Related Blindness (FARB) Laboratory, Biomedical Research Institute, Seoul National University Hospital, and Department of Ophthalmology, Seoul National University College of Medicine, Seoul 03080, Republic of Korea. E-mail: steph25@snu.ac.kr; or Young-Ger Suh, College of Pharmacy, CHA University, Pocheon-si 11160, Republic of Korea; College of Pharmacy, Seoul National University, Seoul, 08826, Republic of Korea. E-mail: ygsuh@cha.ac.kr